

A new atomic force microscope probe with force sensing integrated readout and active tip

A. G. Onaran, M. Balantekin, and W. Lee

G. W. Woodruff School of Mechanical Engineering, Georgia Institute of Technology, Atlanta, Georgia 30332

W. L. Hughes and B. A. Buchine

School of Material Science and Engineering, Georgia Institute of Technology, Atlanta, Georgia 30332

R. O. Guldiken and Z. Parlak

G. W. Woodruff School of Mechanical Engineering, Georgia Institute of Technology, Atlanta, Georgia 30332

C. F. Quate

E. L. Ginzton Laboratory, Stanford University, Stanford, California 94305

F. L. Degertekin^{a)}

G. W. Woodruff School of Mechanical Engineering, Georgia Institute of Technology, Atlanta, Georgia 30332

(Received 13 November 2005; accepted 19 December 2005; published online 9 February 2006)

We introduce a novel probe structure for the atomic force microscope. The probe has a sharp tip placed on a micromachined membrane with an integrated displacement sensor, a diffraction-based optical interferometer. We use this probe in a microscope to directly measure the transient interaction forces between the probe tip and the sample when operating in a dynamic mode. We form images related to viscoelasticity and adhesion of the samples by recording salient features of individual tap signals. We also produce tapping mode images of sample topography an order of magnitude faster than current probe microscopes using an integrated electrostatic actuator to move the probe tip. We envision a broad range of applications for this device that range from life sciences to microelectronics. © 2006 American Institute of Physics. [DOI: [10.1063/1.2166469](https://doi.org/10.1063/1.2166469)]

I. INTRODUCTION

Since its invention in 1986,¹ the atomic force microscope (AFM) and its variations have been used to probe a wide range of physical and biological processes, including mechanical properties of single molecules,^{2,3} electric and magnetic fields of single atoms and electrons.^{4–6} Moreover, cantilever-based structures inspired by the AFM have been a significant driver for nanotechnology resulting in chemical sensor arrays,⁷ various forms of lithography tools with high resolution,^{8–10} and terabit level data storage systems.^{11,12} Despite the current rate of success, the AFM clearly needs to be improved in terms of speed, sensitivity, and an ability to generate quantitative data on the chemical and mechanical properties of the sample.

The main function of any probe microscope is to measure the interaction forces when a sharp probe tip is brought close to or in contact with the sample. The attractive and repulsive forces experienced by the AFM tip yield a wealth of information on various surface forces and sample properties.¹³ Several AFM methods, such as nanoindentation,¹⁴ force modulation, ultrasonic AFM,^{15,16} pulsed force mode,¹⁷ and dynamic force spectroscopy¹⁸ have been developed to characterize the viscoelastic properties of the material under investigation. The phase of higher-order vibrations of the AFM cantilever in noncontact mode is pro-

posed to map certain surface properties.¹⁹ Dynamic operation of AFM, such as the tapping mode, eliminates shear forces during the scan, and therefore has advantages in terms of speed and damage to the sample during material property measurement. In this mode, the only free variable, the phase, is related to the energy dissipation but it is difficult to interpret.^{20,21} The inverse problem of gathering the time-domain interaction forces from tapping signal is not easily solvable due to complex dynamics of the AFM cantilever.²² Harmonic imaging is useful to analyze the sample elastic properties since it recovers part of the tip-sample interaction force frequency spectrum.^{23–25} Several methods have been developed to directly measure the interaction forces by tapping on a sample cantilever.^{26,27} The slow dynamics of the sample cantilever has limited these measurements to time average rather than the transient forces applied to the sample. Current cantilever-based structures for the AFM probes also lack the speed required for some imaging and lithography applications. Imaging systems based on small cantilevers have increased the speed of the AFM at the cost of demanding constraints on optical detection and bulky actuators.^{28,29} Arrays of AFM cantilevers with integrated piezoelectric actuators have been developed for parallel lithography and imaging,³⁰ but the complex fabrication methods have limited the use of this technology.

We have recently introduced a membrane-based force sensor for probe microscopy with electrostatic actuation and integrated optical detection.³¹ This structure was originally developed as an opto-acoustic device for microphone and

^{a)} Author to whom correspondence should be addressed; electronic mail: levent.degertekin@me.gatech.edu

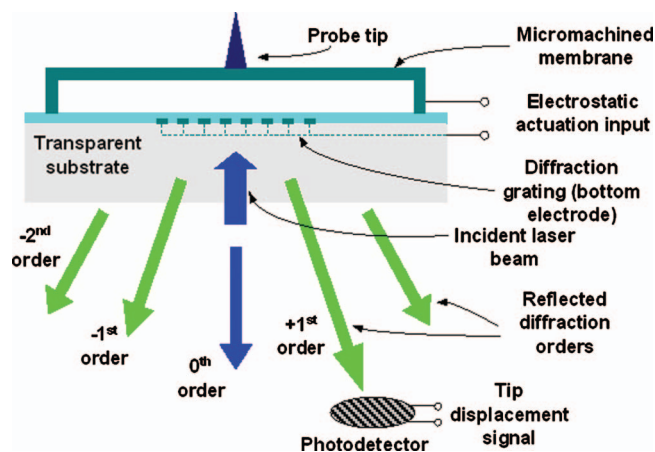


FIG. 1. (Color) Schematic of the FIRAT probe structure and the diffraction-based optical interferometric detection scheme. The transparent substrate is a quartz wafer. One or more diffraction orders can be detected for higher signal and reduced laser noise.

ultrasonic transducer applications.^{32,33} Readout optoelectronics were integrated with a sensor membrane in a volume of 2.5 mm^3 , and near shot noise limited displacement detection with $14 \text{ fm}/\sqrt{\text{Hz}}$ noise level was demonstrated.³⁴ Micromachined dielectric membranes with sealed cavities and embedded separate electrodes for operation in liquid environments were also developed.^{35–37} These membrane structures are suitable for integrated optical or capacitive displacement detection with speeds up to 20 MHz.^{35,38,39} We note that these are different versions of capacitive micromachined ultrasonic transducers,^{35,38,39} and similar membrane structures were proposed for fast tip motion in AFM through integration of sharp tips.⁴⁰

With this background, we integrated a sharp probe tip on the micromachined membrane and transformed the aforementioned optoacoustic device into a novel probe for atomic force microscopy, which we call the force sensing integrated readout and active tip (FIRAT). Using carefully designed micromachined mechanical structures with spring constants in the 1 N/m range and noise levels down to $10 \text{ fm}/\sqrt{\text{Hz}}$, one can achieve piconewton force resolution with 10 kHz measurement bandwidth with this device. In this article, we describe the FIRAT probe structure and operation. We also demonstrate its interaction force measurement capability and use it for material property measurement and imaging. We envision significant advances in probe microscopy in terms of speed, sensitivity, size, quantitative measurements, and scalability for array operation with FIRAT probes.

II. FIRAT PROBE STRUCTURE

The particular version of the FIRAT probe used for our experiments is shown in Fig. 1. The main structure consists of a sharp tip placed on a micromachined, optically reflective, electrically conductive membrane built on a transparent substrate. Underneath the membrane there is a metallic optical diffraction grating deposited on the substrate and covered with a dielectric layer to prevent electrical shorting in case of membrane collapse. This forms an integrated phase-sensitive diffraction grating structure which enables us to measure the

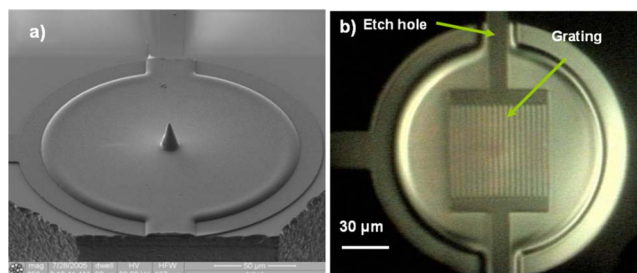


FIG. 2. (a) The FIB micrograph of a FIRAT probe with $150 \mu\text{m}$ diameter aluminum membrane and platinum tip. The 0.5-mm -thick quartz substrate is cut close to the membrane edge to minimize alignment problems with the sample due to parallelism errors. The electrodes on the left and the top are also seen. (b) Optical micrograph of the device from the backside. The grating with $4 \mu\text{m}$ period is connected to external electrical source. Etch holes are also seen.

membrane (probe tip) displacement with the sensitivity of a Michelson interferometer.^{41–43} The displacement of the FIRAT probe tip due to forces acting on it is monitored by illuminating the diffraction grating through the transparent substrate with a coherent light source, and the intensity of the reflected diffraction orders is recorded by photodetectors at fixed locations. The probe's tip is moved by electrostatic forces applied to the membrane using the diffraction grating as an integrated rigid actuator electrode. In applications where an external actuator moves the transparent FIRAT probe substrate this actuator is used to adjust the probe tip position for optimal displacement measurement sensitivity and can oscillate the tip. For applications requiring high speeds, this integrated actuator can be used as the *only* actuator in the feedback loop to move the probe tip with a speed limited by the membrane dynamics.³¹

Figure 2(a) shows a focused ion beam (FIB) micrograph of a typical FIRAT probe structure that we used in our experiments. The $0.9\text{-}\mu\text{m}$ -thick aluminum membrane is $150 \mu\text{m}$ in diameter and fabricated on a 0.5-mm -thick quartz substrate. Figure 2(b) shows the optical micrograph of the microscope membrane from the backside. The grating and the electrical connections are clearly seen as well as the darker spot at the position of the tip at the middle of the membrane. The 90-nm -thick aluminum grating is evaporated over a 30-nm -thick titanium adhesion layer and patterned to have $4 \mu\text{m}$ grating period with 50% fill factor. A 220-nm -thick oxide layer is deposited over the grating using plasma-enhanced chemical-vapor deposition. The static membrane stiffness of a typical membrane was measured to be approximately 133 N/m using a calibrated AFM cantilever. Several tips were fabricated out of platinum and tungsten using a FIB. The process involved ion-beam-assisted chemical-vapor deposition where molecules adsorb on the surface but only decompose where the ion beam.⁴⁴ We fabricated tips with radius of curvatures down to 50 nm on aluminum membranes using this method.

III. EXPERIMENTAL SETUP

We modified a commercial AFM system⁴⁵ for our experiments with the FIRAT probe and monitored the intensity of the $+1^{\text{st}}$ diffraction order as the tip displacement signal. As

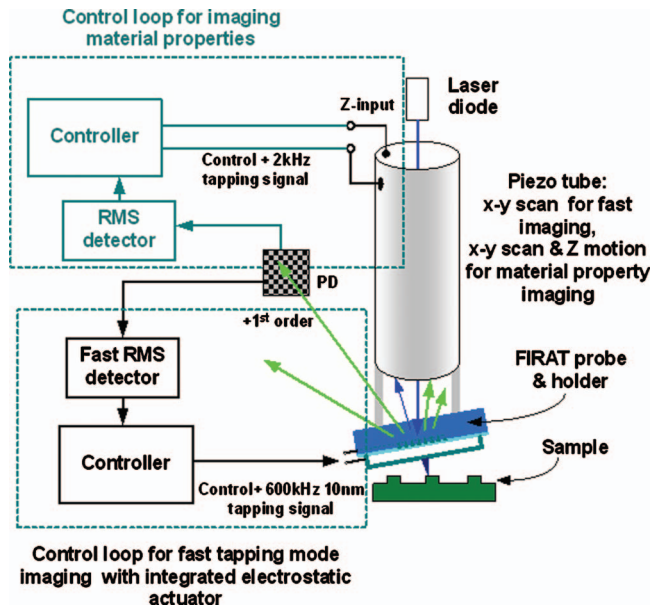


FIG. 3. (Color) Experimental setup integrating the FIRAT probe with a commercial AFM system. A custom-made holder is used to attach the FIRAT probe substrate to the piezo tube at an angle to direct first-order beam to the photodiode. The internal controller of the AFM and a detector for peak force measurement are used for substrate-driven tapping mode. A faster external rms detector is implemented for fast tapping mode imaging.

shown in Fig. 3, we mounted the quartz chip with the FIRAT probe on a custom designed holder for the commercial AFM and monitored the intensity of the $+1^{\text{st}}$ diffraction order as the tip displacement signal. With $4 \mu\text{m}$ grating period and 670 nm laser wavelength, the $+1^{\text{st}}$ diffraction order is reflected at a 9.6° angle from the grating normal. A holder tilted 6.2° with respect to the incident beam provides a total of 22° angular deflection; the same angle as the cantilever-based beam bounce method. Note that with the FIRAT probe all the incident light is reflected from the grating and the membrane, eliminating any optical interference problems due to reflections from the sample; providing a clean background for tip displacement measurements. To characterize the static and dynamic performance of the FIRAT probe system, we used the integrated electrostatic actuator. We traced the optical interference curve with a dc bias range of $24\text{--}36 \text{ V}$ and adjusted the bias for optimum sensitivity point at 30 V . The displacement sensitivity at this bias level was 204 mV/nm . The measured tip displacement noise, confirmed by spectrum analyzer measurements, corresponds to $100 \text{ fm}/\sqrt{\text{Hz}}$ with $1/f$ corner frequency of 100 Hz . Using the laser power available from the zeroth and -1^{st} diffraction order and differential detection, this value can be lowered well below $50 \text{ fm}/\sqrt{\text{Hz}}$ without increasing the laser power or using etalon detection.⁴⁶ The dynamic response of a typical membrane was measured using the integrated electrostatic actuator, indicating a resonance frequency of 720 kHz with a quality factor of 4.1 , suitable for fast tapping mode imaging. We implemented a controller to maintain the rms value of the photodetector signal generated by the FIRAT probe at a constant level when it taps on the sample. For material property measurement and imaging using transient interaction force signals, the Z input of the piezo tube was driven to generate

a 2 kHz sinusoidal signal. The signal frequency is chosen as a compromise between the ability to generate adequate displacement of the Z piezo and the frequency response of the internal RMS detector of the commercial system. The other controller scheme is used for fast tapping mode imaging. In this case, the Z input of the piezo tube is disabled, and the integrated electrostatic actuator is used to generate 10 nm peak to peak-free air FIRAT probe tapping signal in the $500\text{--}700 \text{ kHz}$ range as well as the signals to control the FIRAT probe position keeping the rms value of the tip vibration at the desired set point.

IV. DIRECT MEASUREMENT OF TRANSIENT INTERACTION FORCES

We directly measure time-domain interaction forces as shown in Fig. 4(a). Here, the FIRAT probe substrate oscillates as driven by a suitable actuator. Both the attractive and repulsive regions of the force curve are traced as the probe tip contacts the sample during each cycle. In Fig. 4(a), we show the shape of the FIRAT probe membrane during different phases of a cycle while the FIRAT probe substrate oscillates at 2 kHz . The measured photodetector output signal during that cycle is also shown. During phase I, the FIRAT tip is away from the sample surface (in this case silicon) where it experiences long-range attractive forces. When brought close to the surface, the tip jumps to contact (0.2 nm change in tip position, phase II) and remains in contact for about 14% of the cycle. In the middle of the period, the repulsive force applied to the sample reaches to a peak value of 163 nN (1.22 nm tip displacement, phase III). When the tip is withdrawn, the tip experiences adhesion forces of 133 nN (phase IV) before breaking off from the silicon surface (phase V). As shown in Fig. 4(b), the controller stabilizes the signal with a constant rms, so that the output signal of the FIRAT probe shows individual and repeatable taps on the sample.

An important application of this mode of operation is the measurement of local viscoelastic properties. In Fig. 4(c) we compare individual tap signals obtained on (100)-oriented silicon and photoresist (Shipley 1813) samples using the FIRAT probe tip with 50 nm radius of curvature. The maximum repulsive force is significantly larger for the silicon sample even though the tip-sample contact time is less than that of photoresist (PR). We also used a simple theoretical model using Derjagin-Muller-Toropov (DMT) mechanics and adhesion hysteresis for an initial investigation of the quantitative elasticity measurement potential of this method⁴⁷ (Appendix A). The results of simulations for this particular case are shown in Fig. 4(c). Simulated tap signals for silicon with $E=117 \text{ GPa}$ (taken as a reference material), and $E=10 \text{ GPa}$ for PR agree well with the measured individual tap signals, and the expected value of $E \sim 7\text{--}20 \text{ GPa}$ for a typical positive photoresist film.⁴⁸ We also note the higher capillary hysteresis observed on the silicon sample. Both of these results are consistent with existing models and data obtained by others.^{22,49}

These results clearly demonstrate the unique feature of the FIRAT probe for dynamic force measurements: The output signal is generated only when there is an interaction

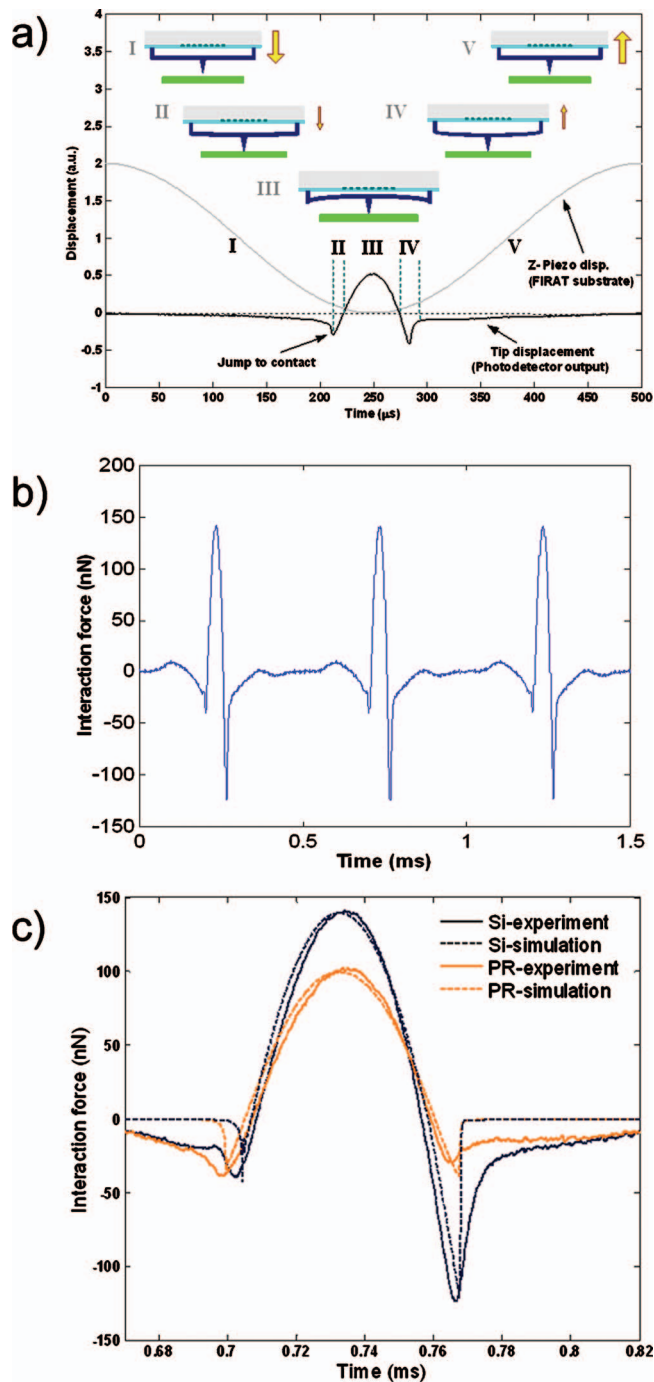


FIG. 4. (Color) (a) The shape of the FIRAT probe during different phases of a cycle of the substrate-driven tapping mode. The size and direction of the arrows indicate the speed and direction of motion of the FIRAT probe substrate. The substrate position and the FIRAT probe output signals are also shown. (b) Individual tap signals during three tapping cycles. (c) Measured and simulated interaction forces during a single tap on PR and silicon. The slope, contact time, and differences in attractive forces form material signatures, and can be used for quantitative inversion of material and surface properties.

force on the probe tip. With broad bandwidth and high sensitivity, the FIRAT probe enables direct measurement of transient interaction forces during each *individual tap* with high resolution and *without background signal*. This provides crucial information on properties such as adhesion, capillary forces, as well as sample viscoelasticity. To the best of our

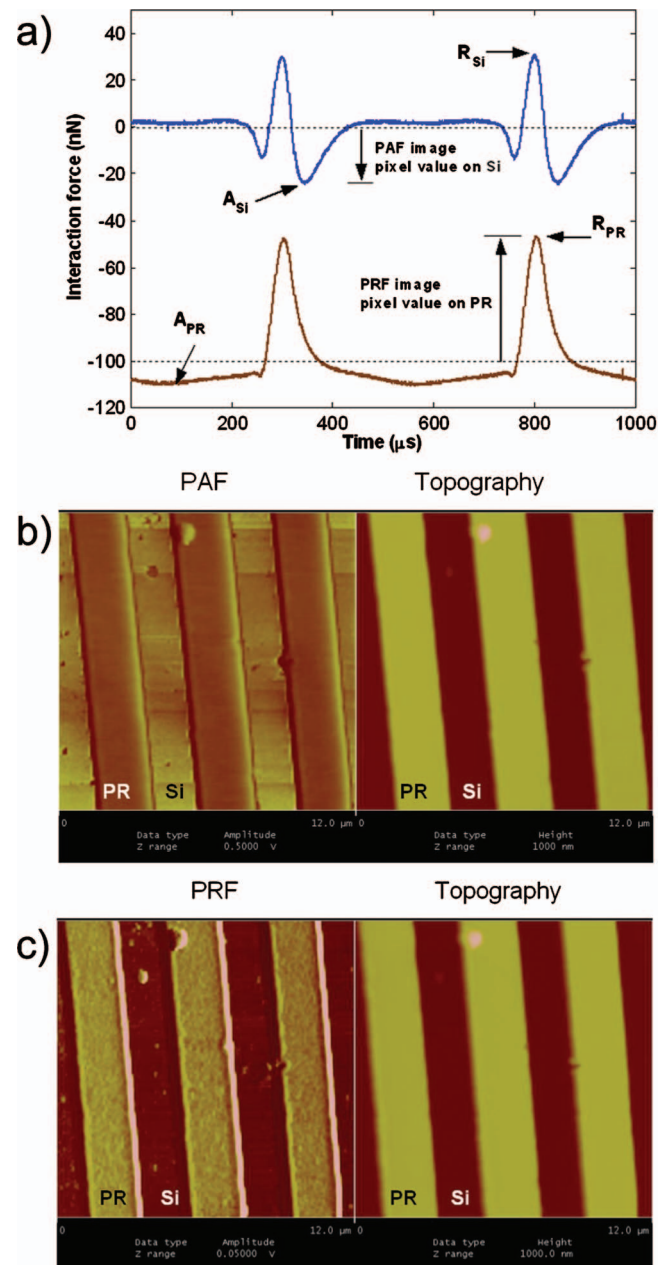


FIG. 5. (Color) (a) Measured interaction force signals on silicon (blue:top) and 360-nm-thick PR (red:bottom) regions of the sample. (b) Simultaneous PAF (left) and topography (right) images of the sample effectively showing the adhesion map of the sample. (c) Simultaneous PRF (left) and topography (right) images which provide information on sample viscoelasticity.

knowledge, this is the first demonstration of a probe microscope with this capability.

V. MATERIAL PROPERTY IMAGING

Having access to the transient interaction force, we used the FIRAT probe to image different material properties by recording at each pixel the salient features of the tap signal. Figure 5(a) shows the transient tap signals on the PR and silicon regions of a sample that consists of 360-nm-thick, 2- μm -wide PR strips with 4 μm periodicity patterned on the silicon substrate. There are significant differences between the tap signals in terms of both the attractive and repulsive forces acting on the probe tip. The silicon surface exhibits

much larger adhesion force as compared to the PR surface. Since the controller tries to maintain a constant rms value, it forces the FIRAT probe to indent more into the PR region, thus the tip experiences a larger repulsive force. Note that the shape of the individual tap signals in the attractive region has strong dependence on the environment. This data set was taken at a later time, with a larger FIRAT probe tip (radius ~ 150 nm) on a different sample as compared to Fig. 4.

To form an image in which sample adhesion dominates the contrast mechanism, we used a peak detector circuit to record the peak attractive force (PAF) as the pixel value [such as points A_{Si} and A_{PR} in Fig. 5(a)]. Simultaneously, we recorded the sample topography by keeping the rms value at a constant level. Figure 5(b) shows the resulting adhesion (PAF) and topography images. In the topography image, the bright stripes correspond to PR (Shibley 1805). In the PAF image the silicon surface appears brighter than PR due to higher adhesion forces. By recording the peak repulsive force (PRF) as the pixel value, we obtained images where sample viscoelasticity dominates the contrast [points R_{Si} and R_{PR} in Fig. 5(a)]. Simultaneously recorded PRF and topography images of the same sample region are shown in Fig. 5(c). The PRF image shows a reversed contrast as compared to the PAF image, while the topography image is repeatable. The PR strips appear brighter in the PRF image as indicated by the individual tap signals shown in Fig. 5(a). We note that many more contamination particles are adhered to the silicon surface. This is consistent with higher adhesion measured on the silicon in the PAF image.

To further demonstrate the ability of FIRAT probe in generating direct information on material and surface properties, we imaged a checkerboard sample consisting of silicon, chromium (Cr), and aluminum (Al) materials as shown schematically in Fig. 6(a). The sample is made by evaporating and patterning first 140-nm-thick, $2\text{-}\mu\text{m}$ -wide chromium (Cr) lines on silicon substrate and then 150-nm-thick Al lines in a perpendicular direction overlapping with Cr lines. Figure 6(b) shows the simultaneous topography and PAF images. The PAF image clearly shows that the presence of three different materials with a high contrast is due to differences in adhesion. It is noticeably harder to detect the topographical contrast along the aluminum lines in the PAF image. Therefore, this image shows that one can extract material specific information from FIRAT probe tap signals independent of sample topography. We also note in passing that tapping mode phase imaging using a regular AFM cantilever on the same sample did not reveal material-dependent image contrast.

Although we used a simple controller based on the rms value set point for this work, one can use different control schemes by sampling individual tap signals at desired time instants and use those values in the control loop. For example, by keeping the peak value of the repulsive force at a constant level, one can obtain images where the contact time determines the contrast which gives a measure of the sample stiffness. Several existing models can be utilized to convert the data into quantitative material properties.^{25,49-51} Simi-

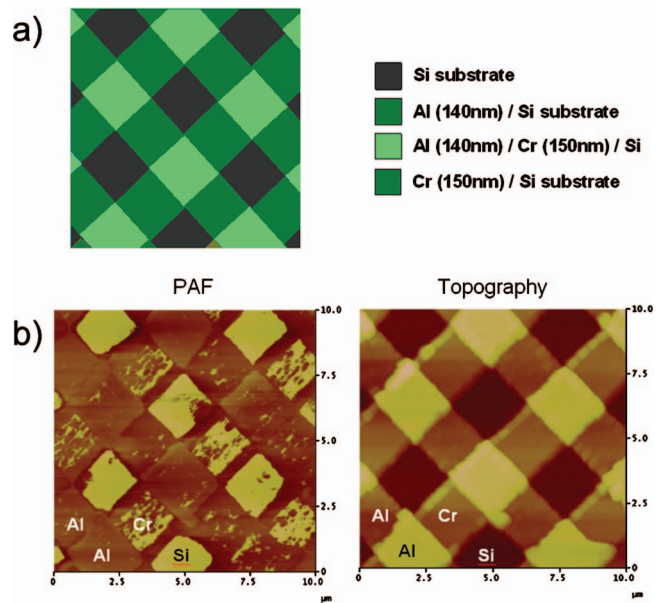


FIG. 6. (Color) (a) Illustration of the imaging sample with three different materials, thin Cr and Al films patterned on silicon substrate. The sample presents same material surface (Al) at different topographical positions as well as two different materials with similar height (Cr and Al). (b) Simultaneous PAF (left) and topography (right) images of the sample effectively showing that FIRAT probe measures the adhesion forces to discriminate between three different material surfaces independent of topography. Images were collected with 0.5 Hz/line scan speed, a tungsten probe tip, and the FIRAT substrate was oscillated at 2 kHz.

larly, by detecting the attractive force peaks before and after the contact one can obtain quantitative information on the hysteresis of the adhesion forces.

VI. FAST TAPPING MODE IMAGING WITH FIRAT PROBE

As shown in Fig. 1, the FIRAT probe has a compact integrated electrostatic actuator, where the electric field between the grating electrodes and the membrane is contained within a closed cavity. This structure can be replicated to form planar arrays of FIRAT probes with good electrical and mechanical isolation.^{35,43} With a suitable set of membrane and electrode materials, it is possible to operate the device in a dielectric or conductive fluid.³⁵ Since the electrostatic forces act only on the probe membrane, the actuation speed as limited by the membrane dynamics is quite fast. Therefore, combined with array operation, the FIRAT probe will be useful for probe microscopy applications requiring high speeds. We have demonstrated the fast tapping mode imaging of sample topography with a single FIRAT probe using the setup shown in Fig. 3. In this mode, the Z input of the piezo tube is disconnected and used only for x-y scan. The integrated electrostatic actuator is used for both oscillating the probe tip at 600 kHz and controlling the membrane bias level in order to keep the oscillation amplitude constant as the tapping mode images are formed.

We use a standard calibration grating with 20-nm-high, $1\text{-}\mu\text{m}$ -wide sharp steps with $2\text{-}\mu\text{m}$ periodicity as the fast imaging sample (NGR-22010 from Veeco Metrology). Figure 7(a) shows the images of a $4\text{-}\mu\text{m} \times 250\text{-nm}$ area (512

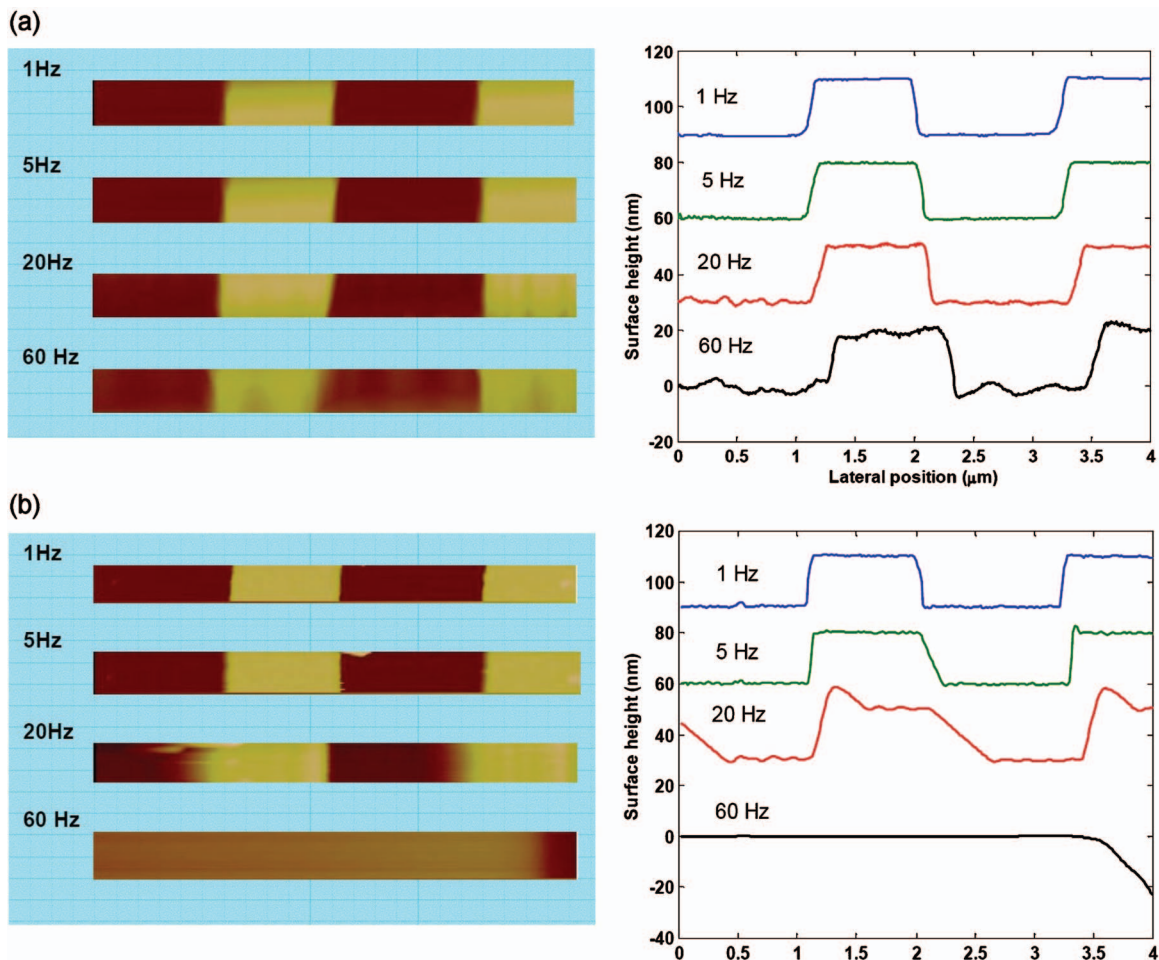


FIG. 7. (Color) (a) Left: topography images of the 20-nm-thick steps of the calibration grating at different imaging speeds as measured by using the integrated electrostatic actuator of the FIRAT probe for Z motion. Right: line scans of the sample at different speeds. (b) Left: topography images of the same sample with a tapping mode cantilever and actuator of the commercial AFM system. Right: line scans of the sample using the AFM cantilever.

$\times 16$ pixels) of the grating with line scan rates of 1, 5, 20, and 60 Hz. Also shown are the cross sections of individual scan lines for each image. The shape of the steps is distorted by the nonsymmetric geometry of the tip. The size of the images and the sample height is limited by the sample alignment and FIRAT tip actuation and detection range of the particular device setup. The commercial AFM instrument that we used limited the maximum x - y scan rate to 60 Hz. For comparison, in Fig. 7(b), we show the tapping mode images and line scans of the same sample obtained using the commercial AFM system and a silicon tapping mode cantilever with a 300 kHz resonance frequency (TESP-A from Veeco Metrology). In this case, the tapping piezo on the cantilever holder was used as the actuator. The FIRAT probe is able to resolve the grating with a 20 Hz line scan rate while some artifacts do appear in the 60 Hz image due to the limited imaging bandwidth. The commercial AFM system is not able to follow the sharp steps starting 5 Hz, and fails to produce a viable image after 20 Hz line scan rate, due to the piezo tube actuator. The imaging bandwidth of the FIRAT probe system controller was about 6 kHz,⁵² limited by the complex dynamics of the air flow in and out of the etch holes on two sides of the membrane [Fig. 2(b)].⁵³ With a sealed cavity, the imaging bandwidth of this particular FIRAT probe

could be increased to 60 kHz with rms detection. Moreover, since FIRAT probe structure is inherently a well-damped system even in air, methods other than RMS detection can be used to implement faster controllers.

VII. CONCLUSION

We have demonstrated the FIRAT probe structure for atomic force microscopy. This probe can perform as an atomic force microscope probe for imaging and offers the unique capability for measuring dynamic interaction forces at a high speed. Although we used a particular implementation of this probe with an integrated optical interferometer, various integrated readout techniques including capacitive, piezoelectric, or piezoresistive could be used. Similarly, the actuator could be a thin-film piezoelectric, a magnetic, or a thermal actuator. We envision FIRAT probes with multiple tips where several sensing and actuation functions are implemented in the same device; where electrical measurements, chemical measurements, information storage, and nanoscale manipulations are performed; all while simultaneously obtaining topography images of the sample in gas or liquid media. This novel probe structure and the method of imaging introduced here open a new area in the field of probe micros-

copy. This new device will enable high-speed imaging and provide images of elastic properties and surface conditions of the sample under investigation.

ACKNOWLEDGMENTS

We thank Dr. Z.L. Wang for his help with the platinum tip fabrication and Mr. Hamdi Torun for his help with sample fabrication. The U.S. National Science Foundation [Grant No. ECS-0348582 to one of the authors (F.L.D.) and Grant No. PHY-0425897 to another author (C.F.Q.)] and the National Institutes of Health [Grant Nos. R01-HL70531 and R56-AI060799 to one of the authors (F.L.D.)] provided the financial support for this research.

APPENDIX

Modeling of FIRAT tip-sample interaction

In our model, we employed DMT contact mechanics and adhesion hysteresis. We also included van der Waals forces to account for attractive surface forces before the contact. Assuming a sphere-flat geometry, the van der Waals (F_{vdW}) and contact (F_{DMT}) forces can be expressed as a function of distance D as⁴⁷

$$F_{\text{vdW}} = -HR/(6D^2), \quad (\text{A1})$$

$$F_{\text{DMT}} = (4/3)E^*R^{1/2}(D_0 - D)^{3/2} - 4\pi R\gamma, \quad (\text{A2})$$

where H is the Hamaker constant, R is the tip radius, E^* is the effective tip-sample elasticity, D_0 is the intermolecular distance, and γ is the surface energy. E^* is given by

$$E^* = [(1 - \nu_{\text{tip}}^2)/E_{\text{tip}} + (1 - \nu_{\text{sample}}^2)/E_{\text{sample}}]^{-1}, \quad (\text{A3})$$

where ν and E are the Poisson ratio and Young's modulus. We used two different γ during the advancing (γ_A) and receding (γ_R) phases to simulate the experimentally observed hysteresis.

The simulation data for silicon sample ($E_{\text{Si}}=117$ GPa, $\nu_{\text{Si}}=0.27$) and a platinum tip ($E_{\text{Pt}}=168$ GPa, $\nu_{\text{Pt}}=0.38$, $R=50$ nm) is obtained with a peak oscillation amplitude of 33 nm. The surface energies for silicon are found to be $\gamma_A=40$ mJ/m² and $\gamma_R=112$ mJ/m². With the same oscillation amplitude, the simulation data for photoresist sample are obtained by using $\gamma_A=\gamma_R=35$ mJ/m² and $E^*=10$ GPa which implies that $E_{\text{Pr}} \approx 10$ GPa.

- ¹G. Binnig, C. F. Quate, and C. Gerber, *Phys. Rev. Lett.* **56**, 930 (1986).
- ²B. T. Marshall *et al.*, *Nature (London)* **423**, 190 (2003).
- ³C. Bustamante, S. B. Smith, J. Liphardt, and D. Smith, *Curr. Opin. Struct. Biol.* **10**, 279 (2000).
- ⁴F. J. Giessibl, S. Hembacher, H. Bielefeldt, and J. Mannhart, *Science* **289**, 422 (2000).
- ⁵D. Rugar, R. Budakian, H. J. Mamin, and B. W. Chui, *Nature (London)* **430**, 329 (2004).
- ⁶M. A. Poggi *et al.*, *Anal. Chem.* **76**, 3429 (2004).
- ⁷C. Hagleitner *et al.*, *Nature (London)* **414**, 293 (2001).
- ⁸S. C. Minne *et al.*, *Appl. Phys. Lett.* **73**, 1742 (1998).
- ⁹S. W. Chung *et al.*, *Small* **1**, 64 (2005).
- ¹⁰R. D. Piner, J. Zhu, F. Xu, S. H. Hong, and C. A. Mirkin, *Science* **283**,

- 661 (1999).
- ¹¹E. B. Cooper *et al.*, *Appl. Phys. Lett.* **75**, 3566 (1999).
- ¹²P. Vettiger *et al.*, *IEEE Trans. Nanotechnol.* **1**, 39 (2002).
- ¹³D. Sarid, *Scanning Force Microscopy: With applications to Electric, Magnetic, and Atomic Forces*, 2nd ed. (Oxford University Press, New York, 1994).
- ¹⁴N. A. Burnham, D. D. Dominguez, R. L. Mowery, and R. J. Colton, *Phys. Rev. Lett.* **64**, 1931 (1990).
- ¹⁵K. Yamanaka, A. Noguchi, T. Tsuji, T. Koike, and T. Goto, *Surf. Interface Anal.* **27**, 600 (1999).
- ¹⁶U. Rabe *et al.*, *Surf. Interface Anal.* **33**, 65 (2002).
- ¹⁷H. U. Krottil *et al.*, *Surf. Interface Anal.* **27**, 336 (1999).
- ¹⁸H. Holscher, W. Allers, U. D. Schwarz, A. Schwarz, and R. Wiesendanger, *Phys. Rev. Lett.* **83**, 4780 (1999).
- ¹⁹T. R. Rodriguez and R. Garcia, *Appl. Phys. Lett.* **84**, 449 (2004).
- ²⁰B. Anczykowski, B. Gotsmann, H. Fuchs, J. P. Cleveland, and V. B. Elings, *Appl. Surf. Sci.* **140**, 376 (1999).
- ²¹M. Balantekin and A. Atalar, *Phys. Rev. B* **67**, 193404 (2003).
- ²²M. Stark, R. W. Stark, W. M. Heckl, and R. Guckenberger, *Proc. Natl. Acad. Sci. U.S.A.* **99**, 8473 (2002).
- ²³R. W. Stark and W. M. Heckl, *Rev. Sci. Instrum.* **74**, 5111 (2003).
- ²⁴O. Sahin, C. F. Quate, O. Solgaard, and A. Atalar, *Phys. Rev. B* **69**, 165416 (2004).
- ²⁵M. Balantekin and A. Atalar, *Phys. Rev. B* **71**, 125416 (2005).
- ²⁶S. C. Fain, K. A. Barry, M. G. Bush, B. Pittenger, and R. N. Louie, *Appl. Phys. Lett.* **76**, 930 (2000).
- ²⁷C. M. Su, L. Huang, and K. Kjoller, *Ultramicroscopy* **100**, 233 (2004).
- ²⁸M. B. Viani *et al.*, *J. Appl. Phys.* **86**, 2258 (1999).
- ²⁹T. Ando *et al.*, *Proc. Natl. Acad. Sci. U.S.A.* **98**, 12468 (2001).
- ³⁰S. C. Minne, S. R. Manalis, and C. F. Quate, *Appl. Phys. Lett.* **67**, 3918 (1995).
- ³¹F. L. Degertekin *et al.*, *Appl. Phys. Lett.* **87**, 213109 (2005).
- ³²N. A. Hall and F. L. Degertekin, *Proc.-IEEE Ultrason. Symp.* **1**, 951 (2000).
- ³³N. A. Hall and F. L. Degertekin, *Appl. Phys. Lett.* **80**, 3859 (2002).
- ³⁴W. Lee, N. A. Hall, Z. P. Zhou, and F. L. Degertekin, *IEEE J. Sel. Top. Quantum Electron.* **10**, 643 (2004).
- ³⁵J. Knight, J. McLean, and F. L. Degertekin, *IEEE Trans. Ultrason. Ferroelectr. Freq. Control* **51**, 1324 (2004).
- ³⁶J. McLean, R. Guldiken, and F. L. Degertekin, *Proc.-IEEE Ultrason. Symp.* **1**, 501 (2004).
- ³⁷R. O. Guldiken, J. McLean, and F. L. Degertekin, *IEEE Trans. Ultrason. Ferroelectr. Freq. Control* (to be published).
- ³⁸B. T. Khuri-Yakub *et al.*, *Jpn. J. Appl. Phys., Part 1* **39**, 2883 (2000).
- ³⁹O. Oralkan *et al.*, *IEEE Trans. Ultrason. Ferroelectr. Freq. Control* **49**, 1596 (2002).
- ⁴⁰G. Percin and B. T. Khuri-Yakub, U.S. Patent No. 6,291,927 (2001).
- ⁴¹T. Sulchek *et al.*, *Appl. Phys. Lett.* **78**, 1787 (2001).
- ⁴²G. G. Yaralioglu, A. Atalar, S. R. Manalis, and C. F. Quate, *J. Appl. Phys.* **83**, 7405 (1998).
- ⁴³N. A. Hall, W. Lee, and L. Degertekin, *IEEE Trans. Ultrason. Ferroelectr. Freq. Control* **50**, 1570 (2003).
- ⁴⁴L. A. Giannuzzi and F. A. Stevie, *Introduction to Focused Ion Beams* (Springer, Berlin, 2005).
- ⁴⁵Nanoscope, 3100, Santa Barbara, CA, Veeco Metrology—Digital Instruments.
- ⁴⁶W. Lee, N. A. Hall, and F. L. Degertekin, *Appl. Phys. Lett.* **85**, 3032 (2004).
- ⁴⁷*Handbook of Micro/Nanotribology*, edited by B. Bhushan (CRC, Boca Raton, Florida, 1999).
- ⁴⁸L. Que and Y. B. Gianchandani, *J. Vac. Sci. Technol. B* **18**, 3450 (2000).
- ⁴⁹D. Sarid, T. G. Ruskell, R. K. Workman, and D. Chen, *J. Vac. Sci. Technol. B* **14**, 864 (1996).
- ⁵⁰R. Garcia and A. San Paulo, *Phys. Rev. B* **60**, 4961 (1999).
- ⁵¹O. Sahin and A. Atalar, *Appl. Phys. Lett.* **78**, 2973 (2001).
- ⁵²T. Sulchek, G. G. Yaralioglu, C. F. Quate, and S. C. Minne, *Rev. Sci. Instrum.* **73**, 2928 (2002).
- ⁵³N. A. Hall, Ph.D. thesis, Georgia Institute of Technology, 2004.